Aerosol Science and Technology
Publication details, including instructions for authors and subscription information:
http://www.tandfonline.com/loi/uast20

Fibrous Particle Deposition in a Turbulent Channel Flow—An Experimental Study

William Kvasnak [a] & Goodarz Ahmadi [a]
[a] Department of Mechanical and Aeronautical Engineering , Clarkson University , Potsdam, NY, 13699
Published online: 13 Jun 2007.

To cite this article: William Kvasnak & Goodarz Ahmadi (1995) Fibrous Particle Deposition in a Turbulent Channel Flow—An Experimental Study, Aerosol Science and Technology, 23:4, 641-652, DOI: 10.1080/02786829508965344

To link to this article: http://dx.doi.org/10.1080/02786829508965344

Fibrous Particle Deposition in a Turbulent Channel Flow—An Experimental Study

William Kvasnak and Goodarz Ahmadi
Department of Mechanical and Aeronautical Engineering, Clarkson University, Potsdam, NY 13699

The deposition rate of glass cylinders and dust paper fibers in a turbulent duct flow was studied experimentally. The glass fibers with a minimum diameter of 5 μm and the paper fibers with a minimum diameter of 1–20 μm and aspect ratios from 4 to 20 were deposited on a flat gold plate. The particle concentration at the test section was measured with the aid of an isokinetic probe in conjunction with a digital image processing technique. An oil lubricant was used on the plate to reduce the effect of particle bounce from the surface. The experimental data show that the deposition rate increases with an increase in fiber length and size. For a fixed minimum diameter or a fixed equivalent relaxation time, the deposition rate increases rapidly with fiber aspect ratio. When the equivalent spherical particle relaxation time is used, the deposition rate of the fibers was found to increase only slightly with aspect ratio and resemble those of spherical particles. The measured deposition velocities were in good agreement with the empirical model predictions and previous data.

INTRODUCTION

Particulate transport and deposition are of crucial interest to many industries. Microcontamination due to small particles in microelectronic and imaging industries, coal transport and cleaning, and multifuel rocket engines are but a few examples. Extensive reviews on the subject of aerosol deposition were provided by Wood (1981), Hinds (1982), Hidy (1984), and Papavergos and Hedley (1984). Accordingly, several empirical models for particle deposition rate were developed in the literature. The available experimental data on the subject, however, have been generally limited to spherical particles. Little if any experimental data under controlled condition on the deposition rate of irregular shaped particles and/or fibers was reported.

Experimental studies of aerosol deposition in the horizontal flow configuration were reported by Alexander and Coldren (1951), and Namie and Ueda (1972). Their results showed that the concentration profiles were asymmetric exhibiting a maximum close to the wall. McCoy and Hanratty (1977) also found strongly asymmetric concentration profiles. Montgomery (1969) measured droplet concentration in fully developed horizontal turbulent channel flows. Kvasnak et al. (1993) provided experimental data for deposition rate of glass beads and compact irregular shaped particles in a horizontal wind tunnel under turbulent flow conditions. The gravitational effect on aerosol deposition rate was studied theoretically by Sehmel and Schwendiman (1963), Owen (1969), and more recently by Fan and Ahmadi (1993a).

The deposition rate of elongated particles in laminar flows was studied theoretically and experimentally by Gallily and Eisner (1982), Gallily and Cohen (1979), Schiby and Gallily (1980), Eisner and Gallily (1982), and Krushkal and Gallily (1984, 1988). The deposition rate of fibers in the respiratory tracts of humans and animals was studied theoretically by

Aerosol Science and Technology 23:641–652 (1995)

0278-6826/95/$9.50
SSDI 0278-6826(95)00082-Q

Asgharian and Yu (1988, 1989), Asgharian et al. (1988), and Chen and Yu (1990). Foss et al. (1989) and Schamberger et al. (1990) studied the collection efficiency of elongated particles by spheres. Gradon et al. (1989) studied the collection of fibers by filter elements. Other works dealing with transport and deposition of non-spherical particles were reported by Griffiths and Vaughan (1986), and Griffiths (1987, 1988).

Virtually all earlier works on fiber transport and deposition were limited to laminar flow conditions. Recently, Fan and Ahmadi (1993b) studied the diffusion of ellipsoidal particles in an isotropic pseudo-turbulent flow field. Shapiro and Goldenberg (1993) reported the effect of turbulence on the deposition rate of glass fibers. They studied the effect of gravitational assisted and prohibited deposition in a horizontal pipe at several flow Reynolds numbers from 2900 to 87,000. They found that although the deposition rate increased substantially from that of compact particles, an aerodynamic equivalent diameter may be used to collapse the data to that of the spherical particles.

In this work the deposition rates of glass as well as irregular shaped paper fibers in a horizontal wind tunnel under turbulent flow conditions are studied. The deposition process in this configuration is the consequence of turbulent eddy impaction, interception, and gravitational sedimentation. Using an isokinetic sampling probe and an image processing procedure, the deposition rates of fibers are measured and the results are compared with the experimental data of Shapiro and Goldenberg (1993), and the predictions of an empirical model.

EXPERIMENTAL SETUP

The wind tunnel used in the experiment consists of a 3.2-m-long, horizontal, rectangular smooth aluminum duct with a cross sectional area of 15.25×2.54 cm^2. The width to height aspect ratio of about six provides a roughly two-dimensional flow condition near the centerline of the channel. The test section of the channel is 0.36 m long and is located 2.36 m downstream of the inlet. The tunnel provides the 50 hydraulic diameters needed to ensure a fully developed velocity profile at the test section. The channel used in this study is an upgraded version of the one used in the previous work of Kvasnak et al. (1993) for measuring the deposition rate of compact dust particles.

The air flow in the tunnel is provided by a centrifugal blower driven by an 11-kW, three-phase, ac motor connected to a digital voltage inverter. The blower is capable of providing a wide range of test section velocities from 1.3 to over 60 m/s. The inverter allows for the variation of frequency input to the motor for controlling its power and rpm. The blower motor combination sits on a one ton weight, reinforced concrete block, and has very little vibration even at an exceedingly large rpm. The blower exits into a 0.61 m long diffuser. The side walls of the diffuser are at an angle of 4.2 degrees to the horizontal axis, and the top and bottom walls are at 7.3 degrees to the same axis. The end of the diffuser contains a HEPA filter which is 99.9999% efficient in the removal of 0.10-μm particles. This filter serves as a flow straightener, as well as filtering any unwanted particles.

A mixing box is used to create a homogeneous aerosol while breaking up any blower generated streamwise vorticies in the air flow. A fourth-order contraction section (shape derived using two fourth order polynomials matched asymptotically at the midpoint) reduces the cross sectional area of the flow by a twelve to one ratio. This provides a flat profile at the inlet of the channel. A grid is placed between the mixing chamber and the contraction section for generating a homoge-

neous turbulence. Another HEPA filter is located at the end of the channel to filter the aerosol and to prevent any back pressure fluctuations in the velocity. Figure 1a shows a schematic of the experimental setup.

The aerosol used in the experiments is generated by an aspirator driven by a compressed air jet which breaks up agglomerates and provides a roughly homogeneous aerosol. The aspirator is a laboratory fabricated device that uses high-velocity air flow in a venturi shaped duct to provide the vacuum needed for entraining the powder. The aspirator suction draws in the dry particles and injects them vertically into the mixing box of the wind tunnel. The turbulent eddies generated by the mixing box disperse the particles into a homogeneous aerosol. The large scale eddies are then broken up by a layer of screens before the tunnel is contracted into the channel. At the test section the particles are deposited onto removable gold plated tiles which are flushly mounted to the lower wall of the channel.

In order to obtain representative samples of the particle concentration at the test section, an isokinetic sampling method is used. A specially designed glass vacuum tube is used to establish the isokinetic environment. Figure 1b shows a schematic of the isokinetic probe mounted in the test section of the tunnel. The inlet of the probe is a 3.2 mm (inside diameter) stainless-steel tube that has been sharpened. The steel tube is connected to a glass tube that diverges into a cone shape with a base diameter of 37 mm and a height of 152.5 mm. The bottom half of the probe houses a piece of porous glass with 60-μm pores. This supports a 37-mm-diameter Millipore, polycarbonate membrane, filter. The filter is a two-dimensional film with a pore size of 0.2 μm. A vacuum pump and a flow meter are connected to the exit tube of the probe and are set to provide the appropriate volumetric flow rate needed to establish the isokinetic environment.

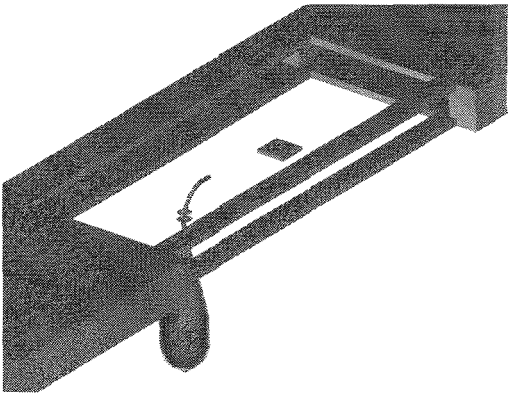

FIGURE 1B. Test section with isokinetic probe and gold plate.

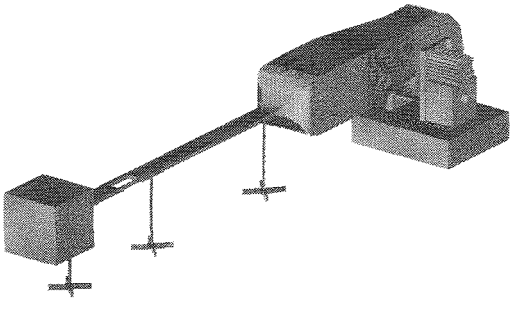

FIGURE 1A. Wind tunnel geometry.

MEASUREMENT PROCEDURE

The procedure used in this experiment is identical to the one described by Kvasnak et al. (1993). The isokinetic probe center line was placed at 5.0 mm from the lower wall of the channel. The vacuum pump attached to the probe was set to ensure that the velocity at the inlet of the probe was equal to the local mean velocity of the unobstructed channel. A suction flow

rate of 1.1 L/min was needed to sustain a mean velocity of 5 m/s at the probe inlet.

According to the data reported by Hetsroni (1982), an aerosol particle concentration of less than 1% by weight may be used to avoid a significant alteration of the undisturbed turbulent flow field. Use of higher concentration levels may lead to substantial modification of the structure of turbulence. The aerosol used in the experiment was generated by dispersing approximately 1 gram of glass or 0.02 grams of paper fibers over a duration of 10 s. This corresponds to a loading less than 0.2% which is by far smaller than the 1% limit. The test section concentration was sampled over a 1-min time span, and the particles deposited on the filter in the isokinetic probe were analyzed by the image processing procedure described in detail by Kvasnak et al. (1993). Thirty digital images having an area of 480 μm by 512 μm were averaged for each particle size with a band width of ± 1.0 μm. The mean concentration at the test section C_0 was given by

$$C_0 = \frac{N_f}{A_{\text{image}}} \frac{A_{\text{filter}}}{A_{\text{probe}}} \frac{1}{Vt}, \tag{1}$$

where N_f is the average number of particles on the image, A_{image}, A_{filter}, and A_{probe}, are the areas of the image, filter, and probe inlet respectively, V is the air velocity at the probe inlet, and t is sample time duration.

Deposition Velocity

The average deposition velocity of particles on the gold plate over a period of 1 min was evaluated in these experiments. The deposition velocity is defined as the flux of particles to the wall over the concentration of the free stream. That is,

$$u_d = \frac{J}{C_0}, \tag{2}$$

where u_d is the deposition velocity, J is the flux of particles to the wall, and C_0 is the free stream concentration. It is assumed that the two dimensionality of the flow allows the particles to deposit uniformly on the channel wall so that any area provides a representative statistical sample. The particle flux J (number deposited per unit area per unit time) to the wall may be evaluated as

$$J = \frac{N_w}{A_{\text{image}} t}, \tag{3}$$

where N_w is the number of deposited particles on the wall in an image, and A_{image} is the area under the microscope. From Eqs. 1–3, it follows that

$$u_d = \frac{N_w V A_{\text{probe}}}{N_f A_{\text{filter}}}. \tag{4}$$

When the air velocity is known, Eq. 4 implies that the deposition velocity may be evaluated directly by counting the number of particles that are deposited on the filter of the isokinetic probe and on the test specimen.

The nondimensional deposition velocity u_d^+ is defined as

$$u_d^+ = \frac{u_d}{u^*}, \tag{5}$$

where u^* is the friction velocity defined as

$$u^* = \sqrt{\frac{\tau_w}{\rho}}. \tag{6}$$

Here, τ_w is the wall shear stress and ρ is the density of air. The wall shear stress in the smooth channel is determined by measuring the pressure drop ΔP for a segment l of the tunnel and using the relation

$$\tau_w = \frac{\Delta P(hb)}{2l(h+b)}, \tag{7}$$

where h and b are the height and width of the channel cross section, respectively.

It is customary to present the deposition velocity data in terms of the nondimensional relaxation time defined for spherical particles as

$$\tau_d^+ = \frac{Sd^{+2}}{18}, \tag{8}$$

where the nondimensional particle diameter is given by

$$d^+ = \frac{du^*}{\nu}. \tag{9}$$

Here, S is the particle to gas density ratio, d is the particle diameter, and ν is the kinematic viscosity of air.

For fibers the definition of the relaxation time becomes a little more complicated. The relaxation time based on the minimum diameter, τ_d^+, may be defined by Eqs. 8 and 9 with $d = 2a$, where a is the minimum radius of the fiber. The fiber is then characterized by τ_d^+ and aspect ratio

$$\beta = \frac{L}{d}, \tag{10}$$

where L is the fiber length. Shapiro and Goldenberg (1993) used an equivalent relaxation time based on the orientation averaged resistance, τ_{eq}^+. Accordingly, the equivalent relaxation time is defined as

$$\tau_{eq}^+ = \frac{m_p u^{*2}}{\mu\nu}\frac{1}{\overline{K}}, \tag{11}$$

where m_p is the mass of the particle, μ is the coefficient of viscosity of air, and

$$\overline{K} = 3\left(K_{xx}^{-1} + K_{yy}^{-1} + K_{zz}^{-1}\right)^{-1}. \tag{12}$$

Here K_{xx}, K_{yy}, and K_{zz} are the components of the resistance tensor.

For cylindrical fibers (Clift et al. 1978)

$$K_{\hat{x}\hat{x}} = K_{\hat{z}\hat{z}} = \frac{4\pi L}{[\ln(2\beta) + 1 - \kappa]}, \tag{13}$$

$$K_{\hat{y}\hat{y}} = \frac{2\pi L}{[\ln(2\beta) - \kappa]}, \tag{14}$$

where $\kappa = 0.80685$. The equivalent relaxation time τ_{eq}^+, is then given by

$$\tau_{eq}^+ = \frac{3}{2}\frac{Sd^{+2}}{18}[\ln(2\beta) - \kappa + 0.5]$$
$$= \frac{3}{2}\tau_d^+[\ln(2\beta) - \kappa + 0.5]. \tag{15}$$

For fibers that are ellipsoids of revolution,

$$K_{\hat{x}\hat{x}} = K_{\hat{z}\hat{z}} = 16\pi a(\beta^2 - 1)\Bigg/\left[\frac{2\beta^2 - 3}{\sqrt{\beta^2 - 1}} \times \ln\left(\beta + \sqrt{\beta^2 - 1}\right) + \beta\right], \tag{16}$$

$$K_{\hat{y}\hat{y}} = 8\pi a(\beta^2 - 1)\Bigg/\left[\frac{2\beta^2 - 1}{\sqrt{\beta^2 - 1}} \times \ln\left(\beta + \sqrt{\beta^2 - 1}\right) - \beta\right]. \tag{17}$$

The particle equivalent relaxation time, τ_{eq}^+ then becomes

$$\tau_{eq}^+ = \frac{Sd^{+2}}{18}\frac{\beta \ln\left(\beta + \sqrt{\beta^2 - 1}\right)}{\sqrt{\beta^2 - 1}}$$
$$= \tau_d^+ \frac{\beta \ln\left(\beta + \sqrt{\beta^2 - 1}\right)}{\sqrt{\beta^2 - 1}}, \tag{18}$$

Alternatively, the equivalent volume sphere relaxation time, τ_{vol}^+, may be defined. In the case of the cylindrical glass fibers, equating the volume of the particle to a sphere, it follows that

$$d_e = d\left(\frac{3\beta}{2}\right)^{1/3}, \tag{19}$$

where d is the diameter of the cylinder. The corresponding relaxation time is then given as

$$\tau_{vol}^+ = \tau_d^+\left(\frac{3}{2}\beta\right)^{2/3}. \tag{20}$$

For ellipsoids of revolution, the diameter of the equivalent volume sphere is given by

$$d_e = d\beta^{1/3}, \tag{21}$$

The corresponding relaxation time is then given as

$$\tau_{\text{vol}}^+ = \tau_d^+ \beta^{2/3}. \tag{22}$$

In the experiment the irregularly shaped paper fibers are assumed to be approximately represented by ellipsoids of revolution. The minimum diameter d and the fiber length are evaluated as the minimum and maximum diameters on the image.

Deposition Measurements

The experimental technique utilized in this study is similar to that of Kvasnak et al. (1993), therefore only a general outline is provided here. To measure the flux of aerosol particles to the wall, a clean gold plate which was covered by a thin layer of Krytox oil was flush mounted to the lower wall of the test section in the wind tunnel. The plate was grounded to reduce electrostatic effects. The isokinetic probe with a membrane filter was also used. A specific amount of glass or paper fibers was prepared for the aerosol generation. Under a steady-state air flow condition, the sample particles were dispersed into the wind tunnel with the aid of an aspirator over a duration of about 1 min. Immediately after the run, the millipore filter and the test plate are removed from the probe and the tunnel test section and processed. The deposited particles were statistically analyzed using the image processing procedure described by Kvasnak et al. (1993). Each image is treated as an independent sample, and thirty images are used for obtaining the average deposition rate of fibers of different sizes and aspect ratios. Since the van der Waals force makes the fiber to lay flat on the surface, the maximum and minimum measured dimensions are used as estimates for the fiber length and diameter.

EMPIRICAL RELATIONS

Wood (1981) proposed a simple empirical equation for the deposition rate of spherical particles from turbulent air streams, for the eddy-impaction regime augmented for the gravitational sedimentation, this equation has the form

$$u_d^+ = 4.5 \times 10^{-4} \tau^{+2} + \tau^+ g^+, \tag{23}$$

where the diffusion term for non-Brownian particles is neglected. Here

$$g^+ = \frac{g\nu}{u^{*3}}, \tag{24}$$

where g is the acceleration of gravity. Shapiro and Goldenberg (1993) proposed several equations for predicting the effect of fiber length on the deposition velocity in vertical and horizontal ducts. However, their empirical equations overestimate the data for spherical particles. Here the correction term suggested by Shapiro and Goldenberg to account for the effect of fiber length is superimposed on Wood's equation. The result is a relation which appears to provide the best fit to the experimental data for both spherical and fibrous particles. The resulting equation is given as

$$u_d^+ = 4.5 \times 10^{-4} (\tau_{\text{vol}}^+)^2 + 5 \times 10^{-3} (L^+)^2 + \tau_{\text{vol}}^+ g^+, \tag{25}$$

where $L^+ = Lu^*/\nu$ is the dimensionless particle length. The second term in equation (25) corresponds to the correction of Shapiro and Goldenberg for the gravitationally enhanced deposition. When this effect is neglected, Eq. 25 reduces to Wood's empirical model. It should be noted that the orientation averaged relaxation time may be used in the first term of Eq. 25, however, the relaxation time based on the equivalent volume sphere provides

the best agreement with the dimensional results. Equation 25 may be restated in a more convenient form as

$$u_d^+ = 4.5 \times 10^{-4}(\tau_{\text{vol}}^+)^2 + 9 \times 10^{-2}\left(\frac{\tau_{\text{vol}}^+}{S}\beta^{4/3}\right) + \tau_{\text{vol}}^+ g^+. \quad (26)$$

This form clearly shows the effect of aspect ratio on the deposition velocity. When the aspect ratio is unity (i.e., spherical particles), Eq. 26 reduces to a slightly altered form of Eq. 23. Note that the turbulent inertial-impaction effects (the first term in Eq. 26) is proportional to the square of τ^+ and makes the major contribution to the deposition rate for small particles. However, as aspect ratio increases, the interception effect, which is linear in τ_{vol}^+ may contribute significantly to the deposition process.

Equation 26 may be expressed in terms of the relaxation time based on the minimum diameter, i.e.,

$$u_d^+ = 4.5 \times 10^{-4}(\tau_d^+)^2\beta^{4/3} + 9 \times 10^{-2}\left(\frac{\tau_d^+}{S}\beta^2\right) + \tau_d^+ g^+ \beta^{2/3}. \quad (27)$$

Equation 27 shows the relation, in powers of β, that for a fixed minimum diameter the deposition rate significantly increases with aspect ratio. Using Eqs. 15 or 18, Eq. 27 may be restated in terms of the equivalent relaxation time based on orientation averaged resistance, i.e.

$$u_d^+ = 4.5 \times 10^{-4}\left(\tau_{\text{eq}}^+\right)^2\beta^{-2/3} \times \frac{\beta^2 - 1}{\left[\ln\left(\beta + \sqrt{\beta^2 - 1}\right)\right]^2} + \left[9 \times 10^{-2}\left(\frac{\tau_{\text{eq}}^+}{S}\beta\right) + \tau_{\text{eq}}^+ g^+ \beta^{-1/3}\right] \times \frac{\sqrt{\beta^2 - 1}}{\ln\left(\beta + \sqrt{\beta^2 - 1}\right)}. \quad (28)$$

Note also that Fan and Ahmadi (1993a) developed an elaborated empirical equation for deposition rate in turbulent flow which accounts for the direction of flow, the lift force acting on the particle, and the surface roughness. It is possible to include the effect of particle aspect ratio in their equation to develop a more detailed model, here however the simplified relations given by Eqs. 25–27 are used.

RESULTS

The experimental results for the deposition rates of cylindrical glass fibers and irregular shaped paper fibers are described in this section. The minimum diameters of the glass fibers was 5 μm and the minimum diameter of the paper fibers used vary from 1 to 20 μm. Each set of data displayed is the average of 6 separate experiments with 30 samples per experiment.

Figure 2 shows a micrograph picture of glass fibers on a gold surface. It is observed that the glass fibers have a constant minimum diameter of 5 μm and a wide range of aspect ratios from 1 to over 100. Due to the rather low concentration used, practically no clustering of the deposited fibers on the gold tile or the isokinetic probe filter was observed. In this study the deposition rates for glass fibers with an aspect ratio in the range of 3 and 20 are presented. While their number were few, most fibers longer than 100 μm were found to cross the edge of the images. This could cause considerable inaccuracy and, therefore, such large size fibers were excluded from the present study. Similarly, particles with aspect ratio's smaller than 3 were not included due to the insufficient number of samples.

Figure 3 shows the measured deposition velocities for 5-μm glass fibers deposited on the lower wall of the channel versus the fiber length. The data of

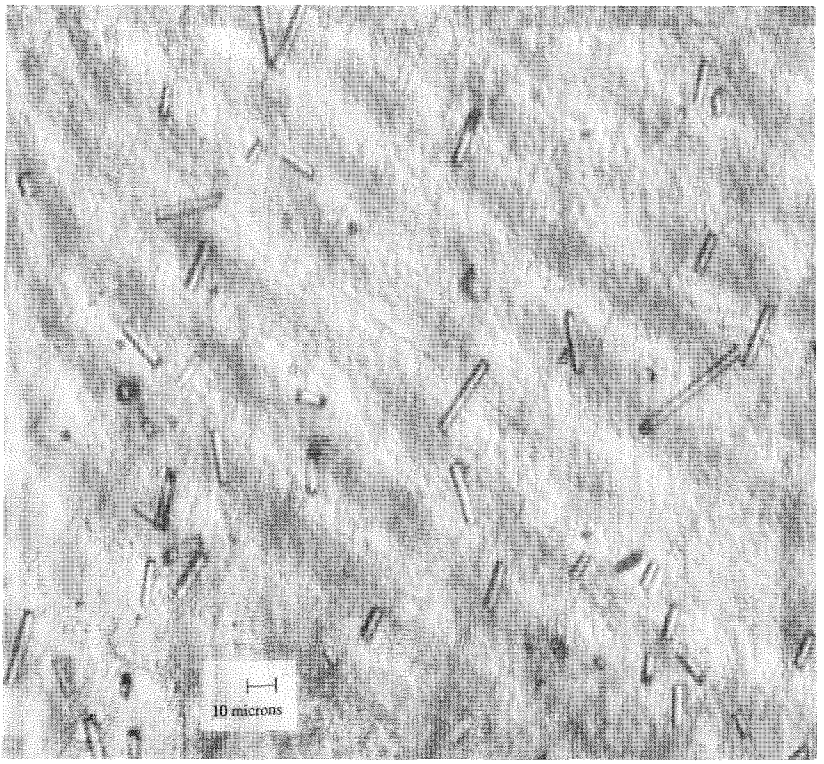

FIGURE 2. Micrograph of glass fibers on gold plate.

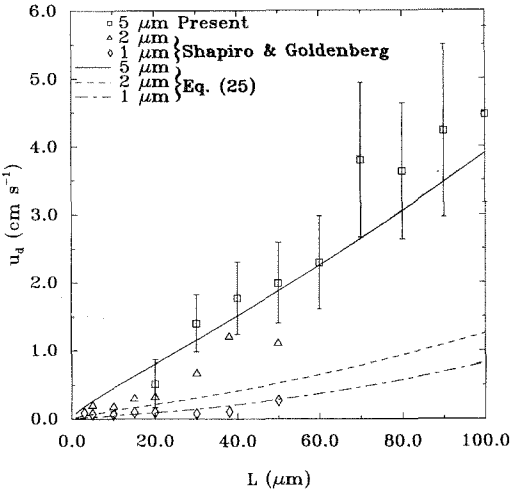

FIGURE 3. Measured deposition velocities of glass fibers.

Shapiro and Goldenberg (1993) for 1 and 2 μm glass fiber deposition are reproduced in this figure for comparison. The predictions of Eq. 25 for different values of diameter are also shown in Fig. 3. A value of $u^* = 0.3$ for the flow conditions in the aerosol wind tunnel is used to express the model predictions in dimensional form. It is observed that the deposition rate increases as the fiber length increases. General agreement is also seen between the empirical model predictions and the experimental data.

Figure 4 shows the nondimensional deposition velocity versus the nondimensional equivalent particle relaxation time, τ_{eq}^+ (based on the orientation averaged resistance). The experimental data of Shapiro and Goldenberg (1993), along with the prediction of the empirical relation given by Eq. 26 are also presented in this figure for comparison. For the empirical model predictions, the minimum diameter of 1, 2, and 5 μm and various aspect ratios are used. Therefore, the increase in τ_{eq}^+ is due to increase of aspect ratio β. A general agreement between the experimental data and the model predictions is observed from this figure. Use of the τ_{eq}^+-scaling in Fig. 4 clearly shows the significant increase of the deposition velocity with aspect ratio of the fiber. This observation is as expected because the increase in aspect ratio increases the wall capture efficiency by the interception mechanism.

Figure 5 shows the nondimensional deposition velocity u_d^+ for 5-μm glass fibers versus the nondimensional equivalent volume spherical particle relaxation time. The data of Shapiro and Goldenberg (1993), the data of Kvasnak et al. (1993) for glass spheres and the predictions of Eq. 26 for different values of β are shown in Fig. 5 for comparison. It is observed that the present data for 5-μm glass fibers are in reasonable agreement with the data of Shapiro and Goldenberg (1993) for 1- and 2-μm fibers. It is observed that the predictions of Eq. 26 for fibers and spherical particles are in reasonable agreement with the experimental data. Furthermore, for a fixed τ_{vol}^+ (i.e. a fixed particle volume), the deposition rate increases only slightly with aspect ratio. As expected, the increasing trend of the deposition velocity with τ_{vol}^+ is clearly observed from Fig. 5.

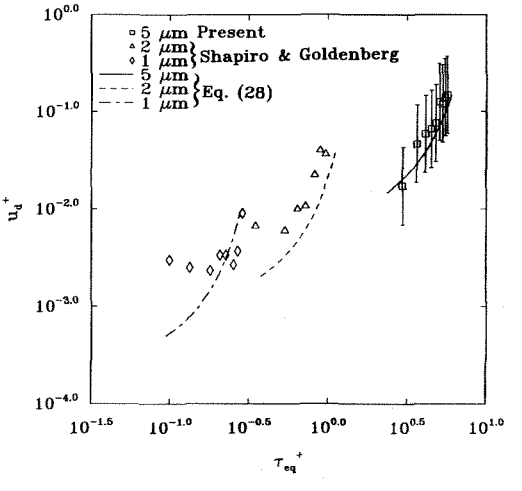

FIGURE 4. Deposition velocities of glass fibers versus τ_{eq}^+ for different minimum diameters.

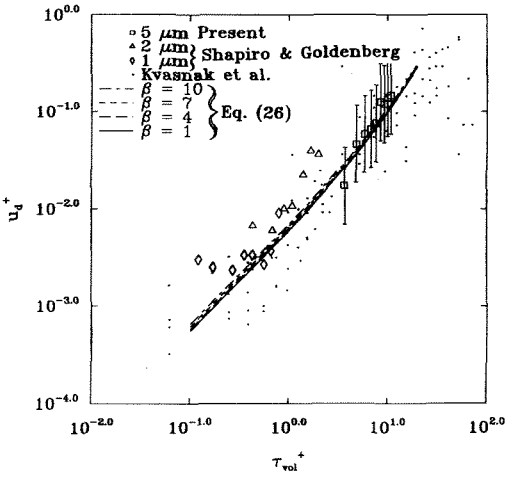

FIGURE 5. Deposition velocities of glass fibers versus τ_{vol}^+

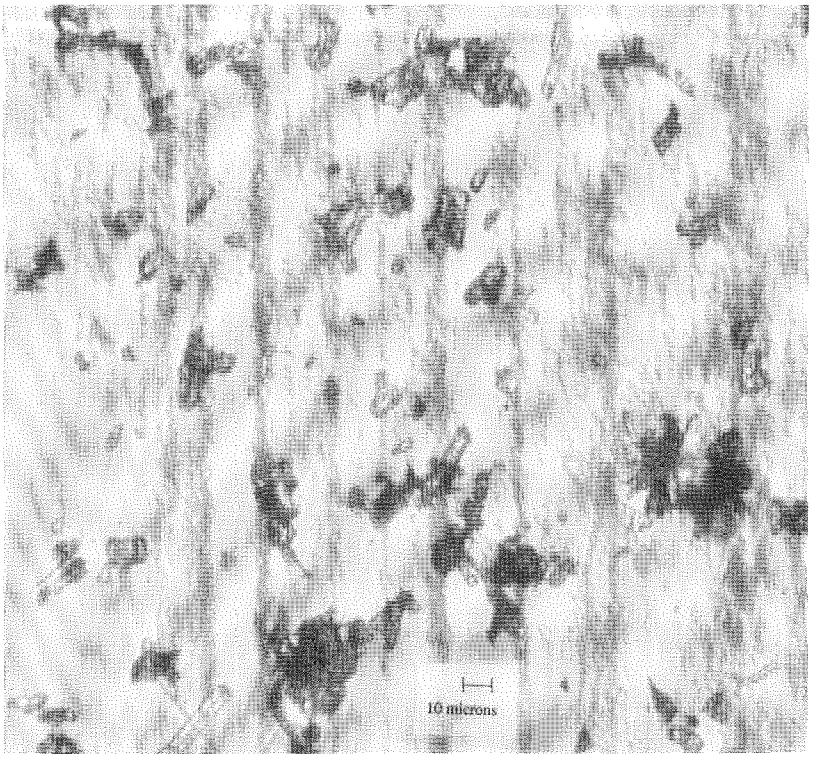

FIGURE 6. Micrograph of paper fibers on gold plate.

Figure 6 shows a micrograph picture of deposited paper fibers on the gold plate. It is observed that the particles are irregular shape and vary in size from 1 to 20 μm with aspect ratios of 3 to 10. In processing of images, the limit on resolution was determined to be about 1.0 μm. Therefore no particles smaller than 1 μm were considered in either the concentration or the deposition measurements. Furthermore, due to the lack of sufficient statistical samples, particles with aspect ratios larger than 10 were also discarded.

Figure 7 shows the nondimensional deposition velocity versus the nondimensional equivalent particle relaxation time (based on the orientation averaged resistance) for the paper fibers. The experimental data of Shapiro and Goldenberg (1993), along with the prediction of the empirical relation given by Eq. 26 for fixed minimum diameter of 1, 2, and 5 μm are presented in this figure for comparison. It is observed that the experimental data for the paper fibers are clustered around those for the 5 μm minimum diameter glass fibers with a few being near the data for the 2 μm glass fibers. Figure 7 also shows reasonable agreement between the experimental data and the model predictions. This figure also indicates the increase of the deposition velocity with particle aspect ratio.

Figure 8 shows the nondimensional deposition velocity of paper fibers versus nondimensional particle relaxation time.

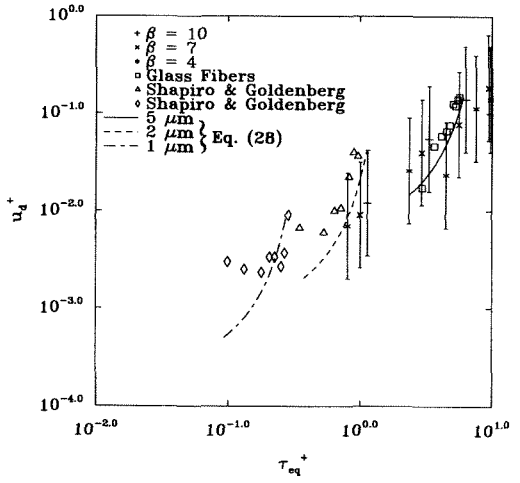

FIGURE 7. Deposition velocities of paper fibers versus τ_{eq}^+ for different effective minimum diameters.

Here τ_{vol}^+, the relaxation time based on the diameter of an equivalent volume sphere as defined by Eq. 22, is used. As noted before, for evaluating the equivalent spherical diameter, a paper fiber was assumed to be an ellipsoid of revolution with diameter and length equal to the shortest and the longest dimensions measured under the microscope. The deposition velocity as evaluated by Eq. 26 are shown in Fig. 8 for comparison. The empirical model predictions appear to be in reasonable agreement with the experimental data for the paper fibers.

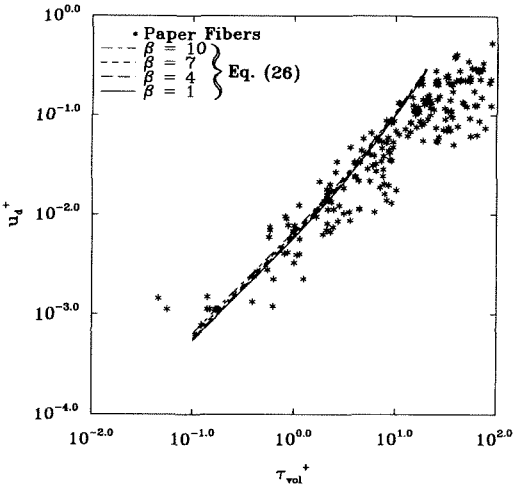

FIGURE 8. Deposition velocities of paper fibers versus τ_{vol}^+

CONCLUSIONS

Based on the presented results the following conclusions concerning fibrous glass and paper particles may be drawn:

1. The deposition rate of 5-μm glass fibers shows a substantial increase with length.
2. The experimental data for deposition rate of glass fibers are in good agreement with the earlier data and the empirical model prediction.
3. Using the equivalent particle relaxation time (based on the orientation averaged resistance), the experimental data show a significant increase with the particle aspect ratio.
4. The fiber deposition rate increases rapidly with aspect ratio for a fixed minimum diameter.
5. For a fixed volume, the fiber deposition rate in a horizontal duct increases only slightly with the aspect ratio.
6. The eddy diffusion-impaction, gravitational sedimentation, and the interception (effective capture radius due to fiber length) mechanisms are important for the deposition of fiber particles larger than 1 μm in turbulent flows.

The authors would like to thank Mr. Raymond Bayer and Mr. Michael Gaynes of IBM Corporation and Dr. Douglas Cooper of Texwipe for many helpful discussions. Early stages of this work was supported by the IBM Corporation and the New York State Center for Science and Technology. The latter stages of this work were supported by the Department of Energy (University Coal Research at PETC) under Grant DE-FG22-94PC-94213, and NASA Marshall Space Flight Center under Grant NGT-51130.

REFERENCES

Alexander, L. G., and Coldren, C. L. (1951). *Ind. Eng. Chem.* 43:1325.

Asgharian, B., and Yu, C. P. (1988). *J. Aerosol Med.* 1:37.

Asgharian, B., and Yu, C. P. (1989). *J. Aerosol Sci.* 20:355.

Asgharian, B., Yu, C. P., and Gradon, L. (1988). *J. Aerosol Sci. Technol.* 9:213.

Chen, Y. K., and Yu, C. P. (1990). *J. Aerosol Sci.* 12:786.

Clift, R., Grace, J. R., and Weber, M. E. (1978). *Bubbles, Drops, and Particles*, Academic, New York.

Eisner, A. D., and Gallily, I. (1982). *J. Colloid Interface Sci.* 88:185.

Fan, F-G., and Ahmadi, G. (1993a). *J. Aerosol Sci.* 24:45.

Fan, F-G., and Ahmadi, G. (1993b). Submitted.

Foss, J. M., Frey, M. F., Schamberger, M. R., Peters, J. E., and Leong, K. M. (1989). *J. Aerosol Sci.* 20:515.

Gallily, I., and Cohen, A. H. (1979). *J. Colloid Interface Sci.* 68:338.

Gallily, I., and Eisner, A. D. (1982). *J. Colloid Interface Sci.* 68:320.

Gradon, L., Grzybowsk, P., and Pilacinsk, W. (1989). *Chem. Eng. Sci.* 43:1253.

Griffiths, W. D. (1987). *J. Aerosol Sci.* 18:761.

Griffiths, W. D. (1988). *J. Aerosol Sci.* 19:703.

Griffiths, W. D., and Vaughan, N. P. (1986). *J. Aerosol Sci.* 17:53.

Hidy, G. M. (1984). *Aerosols*, Academic, New York.

Hinds, W. C. (1982). *Aerosol Technology* John Wiley, New York.

Krushkal, E. M., and Gallily, I. (1984). *J. Colloid Interface Sci.* 99:141.

Krushkal, E. M., and Gallily, I. (1988). *J. Aerosol Sci.* 19:197.

Kvasnak, W., Ahmadi, G., Bayer, R., and Gaynes, M. (1993). *J. Aerosol Sci.* 24:795.

Kvasnak, W. (1991). M.S. thesis, Clarkson University.

McCoy, D. D., and Hanratty, T. J. (1977). *Int. J. Multiphase Flow* 3:319.

Montgomery, T. L. (1969). D.Sc. dissertation, University of Pittsburgh.

Namie, S. and Ueda, T. (1972). *Bull. JSME* 15:1568.

Owen, P. R. (1969). *J. Fluid Mech.* 39:407.

Papavergos, P. G., and Hedley, A. B. (1984). *Chem. Eng. Res. Des.* 62:2755.

Schamberger, M. R., Peters, J. E., and Leong, K. H. (1990). *J. Aerosol Sci.* 21:539.

Schiby, D., and Gallily, I. (1980). *J. Colloid Interface Sci.* 77:328.

Sehmel, G. A., and Schwendiman, L. C. (1963). Hanford Rep Richland Wash.

Shapiro, M., and Goldenberg, M. (1993). *J. Aerosol Sci.* 24:65.

Wood, N. B. (1981). *J. Aerosol Sci.* 12:276.

Received July 26, 1994; revised May 30, 1995